Nitrogen vacancies in InN: Vacancy clustering and metallic bonding from first principles

X. M. Duan and C. Stampfl
School of Physics, The University of Sydney, Sydney, New South Wales 2006, Australia
(Received 13 August 2007; revised manuscript received 28 January 2008; published 20 March 2008)

We perform first-principles density-functional theory calculations to investigate the structural and electronic properties and the formation energies of nitrogen vacancies in wurtzite InN. We report an extensive and systematic study of the favorable atomic and electronic configurations of up to six vacancies in large supercells. The isolated vacancy acts as a donor in a *p*-type material where there is very little interaction between the singly positive charged vacancies. Their spatial distribution is therefore predicted to be random arrangements of single defects. However, in more *n*-type materials, the neutral charge state becomes favored and we find that the vacancies then prefer to be situated close to one another on the nearest-neighbor (like species) sites, forming "vacancy complexes or clusters." In the highest positive charge state of the complexes, the clustering is unstable with respect to isolated single positive charged vacancies. However, the negatively charged and lower positively charged (e.g., 1+ and 2+ charge states for three nitrogen vacancies) complexes also exhibit an attractive interaction between the vacancies, thus also favoring clustering. The formation of such nitrogen vacancy clusters gives rise to local indium-rich regions with metallic-like bonding. We discuss the effect that these defect structures have on the nature of the electronic states in the region of the band gap, in relation to recent experimental results (as measured by, e.g., infrared photoluminescence, x-ray diffraction, and transmission electron microscopy).

DOI: 10.1103/PhysRevB.77.115207 PACS number(s): 71.55.−i, 71.15.Mb, 71.15.Nc, 71.55.Eq

I. INTRODUCTION

In recent years, group III nitrides (GaN, AlN, and InN) and their alloys have attracted significant technical and scientific interest because of their great potential for the development of, and current use in, optoelectronic devices operating in the blue and ultraviolet (UV) regions of the spectrum, which is related to their wide and complementary differences in the fundamental band gap.[1–3] Indium nitride, which is by far the least studied of the group III nitrides, is one of the most "intriguing" semiconductor materials studied up until now. This is the case despite its important role in the active $In_xGa_{1-x}N$ layer in short wavelength light-emitting diodes and laser diodes, whereby increasing the In contents makes it possible to extend the light-emitting range from the UV to the red region. In particular, even the fundamental physical parameters of InN are still under debate: e.g., there has been recent controversy over the band gap of InN, i.e., whether it is around 1.9 eV, as has been widely accepted,[4,5] or closer to 0.7–0.8 eV, as has been experimentally reported[6–8] and obtained from recent first-principles calculations.[9–11] Although some recent experiments[12] report a somewhat larger value of 1.4 eV, *ab initio* calculations in the literature give a wide range of values for the band gap of wurtzite InN depending on the following description: all-electron and pseudopotential calculations including the In 4*d* electrons yield a tiny, no, or negative band gap;[8,13] self-interaction and relaxation corrected pseudopotential calculations give 1.55 eV;[14,15] *GW* calculations yield 0.02 eV;[8] and a value of ~1.4 eV was estimated by using the exact-exchange (EXX) approach.[16] Screened exchange local-density approximation (LDA) calculations report band gaps of 0.8 eV (Ref. 9) and 0.54 eV.[17] More recent first-principles calculations including quasiparticle effects (in combination with other treatments, e.g., self-interaction correction and EXX) report band gaps closer to 0.7–0.8 eV.[10,11] With the nonlinear core correction (nlcc) approach,[18] the band gap is calculated to be 0.65 eV, which is larger than the value with the In 4*d* electrons included in the pesudopotential calculations. We note that it is more usual for the nlcc approach to yield a somewhat larger gap than for treatments that include the In 4*d* electrons. This is due to the absence of repulsion between the metal *d* states and the top valence *p* states of the anion atom at the zone center. [See, e.g., the discussion in Ref. 19. For zinc-blende (cubic) GaN, the band gap obtained using the all-electron full-potential linear muffin-tin orbital approach is 2.0 eV, while the value obtained using the nlcc approach is 2.66 eV.[20] Also, by using the nlcc approach, values of 2.80 and 3.0 eV were reported for the zinc-blende and wurtzite phases of GaN.[21]]

It is thought that the varying experimental values of the band gap is related to the difficulty in producing pure InN; that is, uncontrolled intrinsic (or extrinsic) defects may be the cause of the wide range in experimentally reported band gaps.[22–24] Recent advances in crystal-growth techniques have now opened the door to obtaining higher-quality InN samples[25] and has stimulated new experimental discoveries of this material,[26] which are expected to have a significant impact on device applications involving InN. Much of the work concerning crystal growth and characterization of InN is summarized in recent reviews.[27–29] To date, there are few experimental studies of the defect structures in this material. Nitrogen-rich stoichiometries have been reported to form in InN grown by radio-frequency sputtering,[22] and materials grown by different epitaxy methods have reportedly had inclusions of In metal.[12] In order to control the material properties and ultimately the device characteristics, understanding of the defects (both native and impurity defect complexes) in this interesting and important material is crucial.

In this paper, we have thoroughly investigated the atomic structure, electronic properties, and associated formation en-

ergies of nitrogen vacancies in InN through *ab initio* calculations. Interestingly, we find that in more *n*-type materials, nitrogen vacancies have a tendency to form "clusters" in the neutral, negative, and some positive charge states, while in a *p*-type material, in the highest positive charge state, there is very little interaction between the vacancies, and thus there is no tendency to form clusters. Clustering of nitrogen vacancies leads to a locally indium-rich region, giving rise to defect states with metallic-like bonding.

II. CALCULATION METHOD

Our density-functional theory calculations are carried out using the LDA[30] for the exchange-correlation functional, and the pseudopotential plane-wave method in a supercell geometry with the ESPRESSO code.[31] We use norm-conserving pseudopotentials,[31] including scalar-relativistic corrections, treating the In $4d$ electrons with nlcc, and using an energy cutoff of 60 Ry. A reciprocal space **k**-point mesh of $3\times3\times3$ for all the supercells is employed. We also perform selected calculations that include all electrons[32] for comparison. We use 72-, 96-, and 128-atom wurtzite supercells where all the atomic positions are fully relaxed.

We consider "doping" of up to six nitrogen vacancies (V_N) in the supercell by determining the lowest energy and charge state configurations. The formation energy of the defect system in the charge state q is given by (shown for a single nitrogen vacancy),

$$E^f(V_N^q) = E^{\text{tot}}(V_N^q) - E^{\text{tot}}_{\text{bulk}} + \mu_N + qE_F, \tag{1}$$

where $E^{\text{tot}}(V_N^q)$ is the total energy of the supercell containing the defect in charge state q and $E^{\text{tot}}_{\text{bulk}}$ is the total energy of the supercell of the same size, which contains only bulk material. μ_N is the chemical potential of the nitrogen atom and E_F is the Fermi level, which is chosen to be zero at the valence band maximum, where we properly add a correction term ΔV to align the reference potential in the defect supercell with that in the bulk.[33] We choose In-rich conditions to display our results by setting the indium atom chemical potential to $\mu_{\text{In}}=\mu_{\text{In[bulk]}}$, where $\mu_{\text{In[bulk]}}$ is the chemical potential of the In atom in bulk metal In, and by determining μ_N from the assumption of thermodynamic equilibrium ($\mu_{\text{In}}+\mu_N=\mu_{\text{InN}}$, where μ_{InN} is the chemical potential of bulk indium nitride). N-rich conditions require taking $\mu_N=1/2\mu_{N_2}$, which is the chemical potential of a N atom in the N_2 molecule. μ_{In} is then determined by the above condition for thermodynamic equilibrium. The results of these studies afford the prediction of the lowest energy defects, that is, which nitrogen vacancy configurations and associated charge states are most likely to exist in InN under certain experimental conditions (e.g., nitrogen rich or indium rich and *p* type or *n* type).

Since we also investigate complex formation, we calculate the binding energy, which determines the stability of the defect complex $(X_1X_2\cdots X_N)$ in the charge state q, defined as

$$E_b[(X_1X_2\cdots X_N)^q] = E^f[X_1^{q_1}] + E^f[X_2^{q_2}] + \cdots + E^f[X_N^{q_N}] - E^f[(X_1X_2\cdots X_N)^q], \tag{2}$$

where $q=q_1+q_2+\cdots+q_N$, $E^f[X_1^{q_1}]$, $E^f[X_2^{q_2}]$, and $E^f[X_N^{q_N}]$ are the formation energies of defect X_i in charge state q_i. The sign has been chosen such that a positive binding energy corresponds to a stable bound complex. For the case of a n nitrogen vacancy complex in the $q=n^+$ charge state, this expression simply reduces to $E_b[nV_N^{n+}]=nE^f[V_N^+]-E^f[nV_N^{n+}]$.

III. RESULTS

A. Bulk InN, In, and the N_2 molecule

The optimized wurtzite InN lattice constants are $a=3.511$ Å, $c/a=1.624$, and $u=0.376$, which compare well with the experimental values (i.e., 3.533 Å, 1.611, and 0.375).[34] We calculate the convergence of the heat of formation of InN as a function of cutoff energy, and find that the difference between 50 and 60 Ry is 16 meV but there is only 1 meV between 60 and 80 Ry. We therefore use 60 Ry for our supercell calculations. The heat of formation ΔH_f is calculated to be −1.16 eV. The reported experimental values range from −0.22 to −1.49 eV.[34] The cohesive energy is calculated to be −10.24 eV, where we include the spin-polarization energies of the N and In atoms of 2.925 and 0.076 eV, respectively. The experimental value is −7.97 eV. Thus, the LDA and nlcc approaches overestimate the cohesive energy and heat of formation, as reported in Ref. 35.

The bond length and binding energy of N_2 are calculated to be 1.103 Å and 11.11 eV, respectively, exhibiting the well known overbinding.[35] The experimental values are 1.098 Å and 9.91 eV.[36] Bulk indium crystallizes in a body-centered-tetragonal structure, which corresponds to a distorted face-centered-cubic arrangement. It also undergoes a phase transition to a more close-packed structure depending on the c/a ratio.[37] The cohesive energy of bulk in the body-centered-tetragonal structure is calculated to be −3.52 eV with optimized lattice constants $a=3.011$ Å and $c=4.756$ Å. For these calculations, we used a $6\times6\times6$ **k**-point mesh and an energy cutoff of 60 Ry.[38] All-electron calculations[32] yield −3.25 eV with optimized $a=3.20$ Å and $c=4.905$ Å. The experimental value is −2.52 eV for the cohesive energy[39] with $a=3.24$ Å and $c=4.937$ Å.[40]

B. Single nitrogen vacancy

We first calculate the atomic and electronic structures and the formation energy of the single nitrogen vacancy (V_N). This defect induces defect states in the conduction band occupied by one electron, which is located at the conduction band minimum in the calculations (see Fig. 4). The vacancy thus acts as a single donor. The lattice relaxations around V_N are such that for the neutral state, the four In nearest neighbors are averagely displaced *inward* toward the vacancy by 3.2% with respect to the equilibrium In-N bond length, and for V_N^{+1}, the displacements are *inward* by 1.8%, as shown in Fig. 1.

C. Two and more nitrogen vacancies

We now investigate whether nitrogen vacancies prefer to cluster together, exhibiting an attractive interaction or to be well separated, exhibiting a mutually repulsive interaction. To do this, we consider "vacancy doping" of up to six neutral

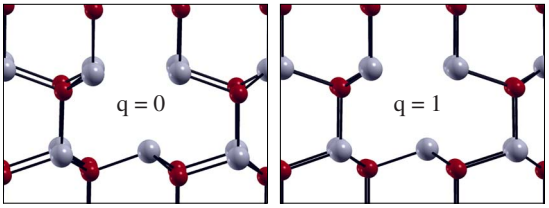

FIG. 1. (Color online) Geometry of the local atomic relaxations around the nitrogen vacancy in the neutral (0) and 1+ charge states q. The pale and dark (red) gray spheres indicate In and N atoms, respectively. The vertical and horizontal directions in the figures are $[0001]$ and $[2\bar{1}\bar{1}0]$ and the axis perpendicular to the paper is $[01\bar{1}0]$.

nitrogen vacancies by performing an exhaustive search for the favored atomic structures. For two and three vacancies, a complete search is carried out in the 72-atom cell, resulting in 7 and 21 atomic configurations, respectively. All clearly favorable configurations are recalculated in a 96-atom cell. Since the most favorable two and three nitrogen vacancy configurations are clearly found to prefer clustering, i.e., to occupy the nearest-neighbor (like species) sites, for the larger vacancy complexes ($n>3$), we tested various configurations by adding the extra vacancy to the most favorable configuration with $n-1$ vacancies in the 96-atom cell. [Note that throughout the paper, we use the term "nearest-neighbor site" where it refers to *like species* sites (i.e., not nearest In-N neighbors).] In all cases, the results show that the nitrogen vacancies prefer to be clustered together, occupying nearest-neighbor [either "in plane," i.e., the vacancies are located in the same (0001) plane, or "out of plane," i.e., the vacancies are located in different (0001) planes] sites. The most favorable structures are then refined in a 128-atom cell. In Table I, we list the energies of the two most favorable structures, as well as the corresponding values for well separated vacancies (for $2V_N$ and $3V_N$). Figure 2 shows the atomic geometries for the two lowest energy vacancy pair configurations, and Fig. 3 shows the lowest energy atomic geometries for the $3V_N$ to $6V_N$ complexes.

For the vacancy pair, the most favorable configuration is where the vacancies are located out of plane on the nearest-neighbor sites (Fig. 2, left). The next most favorable structure consists of the two vacancies on the nearest-neighbor sites in the same (0001) plane (Fig. 2, right), where the energy is 128 meV higher. For the favorable structure, four In-In distances have contracted, resulting in bond lengths very similar to those in bulk In [3.7% (−3.7%) larger (smaller) relative to the calculated (experimental) values]. The favorable out-of-plane vacancy pair induces a number of single defect states in the conduction band region, where one band is doubly occupied, as seen in Fig. 4, which shows the band structure. The defect induced states are indicated in Fig. 4 by the arrows, where all states at and between the arrows, are defect states. We assigned the defect states by plotting the spatial distribution of the square of the wave function at the Γ point. For this vacancy pair, we therefore consider the 1+ and 2+ positive charge states, as well as the 1− and 2− negative charge states, and find that all are stable. With the exception of the single nitrogen vacancy (which has a singly occupied defect state above the conduction band maximum, which is labeled "B" in Fig. 4), all the "vacancy clusters," as for the vacancy pair, can either act as donors or acceptors, as will be seen below. The calculated *binding energy*, however, for the vacancy pair in the 2+ positive charge state shows that the complex is unbound (see Table II), so that it is energetically favorable for the vacancies to exist as singly charged isolated defects. Correspondingly, for the 2+ charge state, there is no contraction of the In-In bonds about the vacancies. Similar to the neutral charge state, there is a contraction of the In-In distances about the vacancies for the negative charge states, resulting in bond lengths that are very similar to those in bulk In [average of 2.0% (−5.3%) larger (smaller) relative to the calculated (experimental) values].

TABLE I. The two lowest energy structures for a given number of nitrogen vacancies V_N and their formation energies E^f per vacancy in the neutral charge state and the energy difference ΔE between them. For two and three vacancies, we also show the least favorable formation energies, corresponding to well separated vacancies denoted as "far," and the energy differences with respect to the most favorable structures. Values in bold indicate the most favorable configuration.

No. of V_N	Configuration	ΔE (eV)	E^f (eV/V_N)
1	–	–	2.15
2	Out-of-plane	0.0	**1.86**
2	In-plane	0.13	1.92
2	"Far"	0.78	2.25
3	Out-of-plane	0.0	**1.75**
3	In-plane	0.14	1.80
3	"Far"	1.50	2.25
4	Rhombus	0.0	**1.56**
4	Pyramid	0.35	1.65
5	Bi-linear	0.0	**1.50**
5	Bi-pyramid	0.18	1.54
6	Bi-linear	0.0	**1.46**
6	Rhombus-pyramid	0.39	1.53

For doping of three vacancies in the neutral charge state, the most favorable configuration is the one where one vacancy is located out of plane and the other two are located in plane, again occupying nearest-neighbor sites [see Fig. 3(a)].

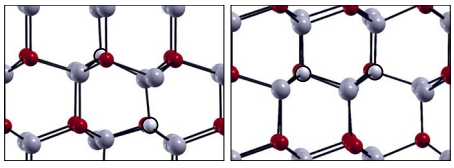

FIG. 2. (Color online) Geometry of the local atomic relaxations around the nitrogen vacancy pair for the most (left) and the next-most (right) favorable configurations. The dark (red) and light gray spheres represent N and In atoms, respectively, and the open circles indicate the V_N sites. The vertical and horizontal directions of the figures are $[0001]$ and $[2\bar{1}\bar{1}0]$ and the axis perpendicular to the paper is $[01\bar{1}0]$.

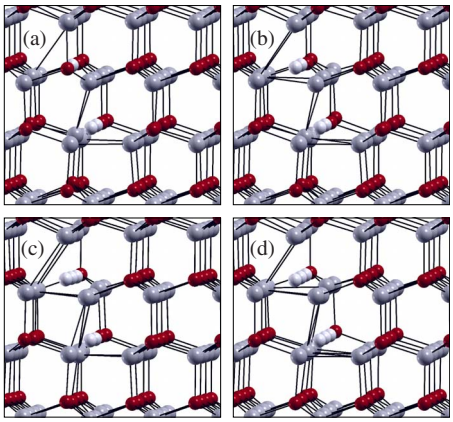

FIG. 3. (Color online) [(a)–(d)] Atomic geometry of the most favorable configurations for three to six nitrogen vacancies in the neutral charge state in InN. The dark (red) and light gray spheres represent N and In atoms, respectively. The vacancy sites are shown as the very pale spheres. Lines joining In atoms indicate that shorter bonds (by a minimum of 8% and a maximum of 14%) have formed compared to the bulk structure.

The next most favorable structure, with an energy that is 140 meV higher, is where all three vacancies are located at the nearest-neighbor sites in the same (0001) plane. For the favorable complex, there is a contraction of five of the In-In distances about the vacancies, again resulting in bond lengths very similar to those in bulk In [average of 3.9% (−3.5%) larger (smaller) relative to the calculated (experimental) values]. This constitutes an average effective inward displacement toward the vacancy of the surrounding In atoms by about 11%. The most favorable $3V_N$ complex induces a number of singlet defect states in the region of the conduction band, one of which is fully occupied by two electrons and another that is occupied by one electron, the rest being unoccupied (see Fig. 4). We therefore consider the 1+, 2+, and 3+ charge states, as well as the 1−, 2−, and 3− negative charge states, and find that all are stable. Similar to the pair vacancy complex, the binding energy of the complex in the highest positive charge state (3+) is not bound, indicating that isolated singly charged vacancies are preferable (see Table II). For all other charge states, the binding energy is positive, indicating that clustering is favorable. Similar to the neutral charge state, there is on average a contraction of five of the In-In distances about the vacancies for the negative charge states, resulting in bond lengths very similar to those in bulk In [average of 3.1% (−4.3%) larger (smaller) relative to the calculated (experimental) values].

For the single, pair, and $3V_N$ vacancy complexes, we carried out some convergence and cross-checks described as follows: Convergence tests for the formation energy of V_N and $2V_N$ shows that the differences between the 96-atom cell and the 128-atom cell are very small: i.e., 0.01 eV in the 1+ charge state for V_N and 0.01 eV for both the neutral and 2+ charge states for $2V_N$. The width of the defect-induced states for $2V_N$ decreases by only 0.018 eV for the 128-atom supercell, as compared to the 96-atom supercell. All-electron

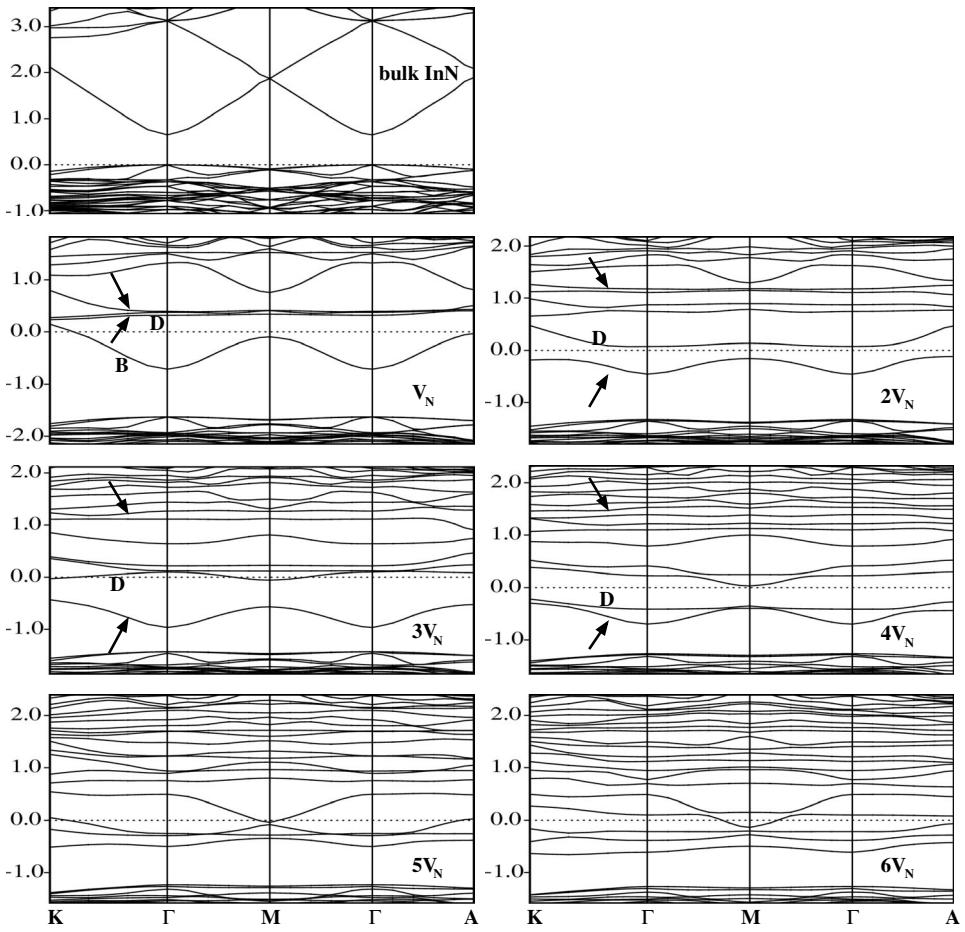

FIG. 4. Band structures for bulk InN and (one to six, V_N to $6V_N$ as labeled) nitrogen vacancies in the neutral charge state in the 128-atom cell. The labels B and D represent bulk and defect states, respectively. The arrows indicate the regions of the defect states; that is, all states between and at the arrows are defect-induced states. The horizontal dotted lines indicate the Fermi level.

TABLE II. The binding energies per nitrogen vacancy E_b/n (in eV) and the average relative displacements $\bar{d}$ (%) of the In atoms neighboring the vacancy site, relative to the bulk In-N bond length, for the defect complexes in various charge states q. A negative number for $\bar{d}$ indicates relaxation toward the vacancy. The binding energies are given with respect to the isolated neutral and single positive charge states for the neutral and positive charge states of the complexes. Since the single nitrogen vacancy does not exist in the single negative charge state, the binding energy of negatively charged complexes is given with respect to the $2V_N^{0,q-}$ and $3V_N^{0,q-}$ complexes.

Configuration	q	E_b/n	$\bar{d}$	q	E_b/n	$\bar{d}$	q	E_b/n	$\bar{d}$
V_N	0	–	−5.07		–		1+	–	−2.06
$2V_N$	0	0.30	−6.93	2−		−8.85	2+	−0.018	−1.56
$3V_N$	0	0.42	−6.43	3−		−6.43	3+	−0.024	−1.11
$3V_N$				2−	0.34	−7.97	2+	0.18	−2.78
$3V_N$				1−	0.25	−7.16	1+	0.35	−5.48
$4V_N$	0	0.59	−6.39	4−	0.43	−8.50	4+	−0.03	0.12
$4V_N$		0		3−	0.45	−7.89	3+	0.15	−2.09
$4V_N$		0		2−	0.40	−7.86	2+	0.32	−3.06
$4V_N$		0		1−	0.38	−6.88	1+	0.48	−4.87
$5V_N$	0	0.67	−6.12	3−	0.42	−7.31	5+	−0.06	−0.50
$5V_N$				1−	0.39	−6.67	3+	0.32	−5.15
$5V_N$							1+	0.57	−2.84
$6V_N$	0	0.70	−5.70	2−	0.52	−6.78	6+	−0.07	0.56
$6V_N$							4+	0.27	−2.29
$6V_N$							2+	0.52	−4.37

calculations using the LDA and the DMOL[3] code with a $2\times2\times2$ **k**-point mesh give a formation energy of 1.39 eV (1.34 eV) in a 72-atom (96-atom) supercell for neutral V_N. For neutral $2V_N$ and $3V_N$, the formation energies are 1.38 eV (1.33 eV) and 1.32 eV (1.32 eV) per vacancy, respectively. The formation energies obtained by DMOL[3] using the generalized-gradient approximation also confirms the clustering tendency of the (neutral) nitrogen vacancies.[41] In general, the formation energies obtained by the all-electron calculations for the neutral nitrogen vacancy clusters ($2V_N$ and $3V_N$) are lower (0.5–0.6 eV) than the present pseudopotential plane-wave calculations using the nlcc approach; this may be due to the overestimation of the cohesive energy of InN in the nlcc approach, i.e., it costs more energy to remove a N atom, and may also be due to the fact that the all-electron calculations yield a smaller band gap so that occupied defect states at or above the conduction band minimum will be at a lower energy. The overall qualitative behavior, however, is reproduced.

For four nitrogen vacancies, clustering is still preferred. The most favorable structure out of a search of nine structures is that where the vacancies form a "rhombus structure," involving two in-plane and two out-of-plane sites [see Fig. 3(b)]. The next most favorable is a "pyramid structure" (one out-of-plane site above three in-plane sites), which is less stable by 0.35 eV. For the favorable complex, there is a contraction of nine of the In-In distances about the vacancies, resulting in bond lengths very similar to those in bulk In [average of 4.1% (−3.3%) larger (smaller) relative to the calculated (experimental) values]. This constitutes an average effective inward displacement toward the vacancy of the surrounding In atoms by about 11%. The rhombus structure complex induces an increased number of defect states in the conduction band region compared to the $3V_N$ and $2V_N$ complexes, where there are two fully occupied singlet states, as well as several unoccupied levels, as seen in Fig. 4. We therefore consider the positive charge states from 1+ to 4+, as well as the negative charge states from 1− to 4−. We find that all charge states except the $2\pm$ charge states are stable. As for the smaller complexes, the binding energy of the highest positive charge state (4+) is negative, showing that it is unbound (see Table II). For all other charge states, the binding energy is positive, indicating that clustering is favorable. For these charge states, there is a contraction of the In-In distances about the vacancies, i.e., on average, 12 of the In-In distances are reduced, resulting in bond lengths very similar to those in bulk In [average of 2.6% (−4.7%) larger (smaller) relative to the calculated (experimental) values].

By adding another vacancy to the most favorable configuration with four vacancies in the 128-atom cell, we find that the most stable structure from a consideration of six configurations is the one where three vacancies are in a line at in-plane sites and the other two in another line at nearest-neighbor out-of-plane sites [see Fig. 3(c)]. The next favorable structure is a symmetric "bipyramid" structure, which is 0.183 eV higher in energy. For the favorable complex, there is a contraction of 11 of the In-In distances about the vacancies, again resulting in bond lengths very similar to those in bulk In [average of 4.8% (−2.9%) larger (smaller) relative to the calculated (experimental) values]. This constitutes an average effective inward displacement of the In atoms by 10% relative to the In-N bulk distance. The most favorable structure induces two fully occupied defect levels and one singly occupied defect level, as well as several unoccupied defect states, as seen in Fig. 4. The number of induced states is

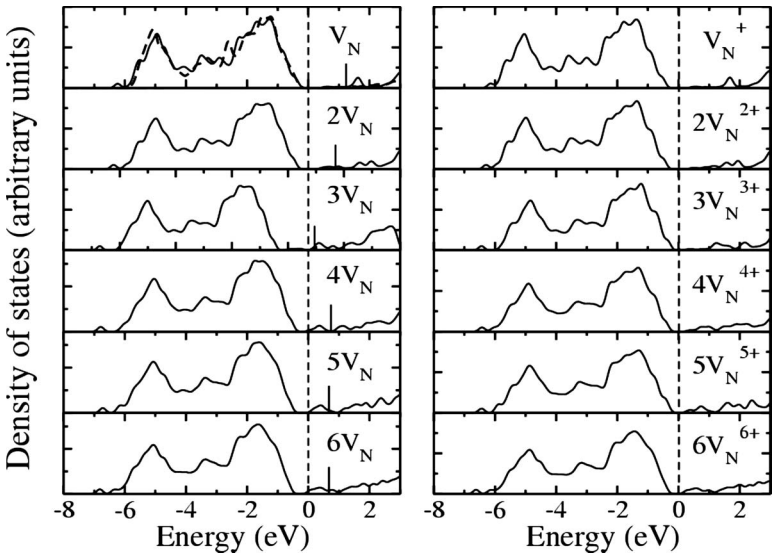

FIG. 5. Total density of states for the most favorable configurations of up to six neutral (left panel) and positive charged (right panel) nitrogen vacancy complexes in wurtzite InN. The dashed lines indicate the valence band maximum (VBM). In the left panel, the short vertical lines indicate the Fermi level. In the right panel, the Fermi level coincides with the VBM. The density of states for bulk InN is included as a dashed line in the neutral isolated nitrogen vacancy plot.

again greater than that for the $4V_N$ and smaller complexes. We consider the (selected) 1+, 3+, and 5+, positive charge states as well as the 1− and 3− negative charge states, and find that all are stable. Again, the highest positive charge state (5+) is unbound. With regard to the lattice relaxations, for the $5V_N$ complex in the negative charge states, they are very similar to the neutral charge state but are slightly more contracted, just as found for smaller complexes. This behavior is also analogous to the $6V_N$, as discussed below.

For the six vacancy complex, we calculated five possible configurations based on the most favorable structure for five vacancy complexes. The most favorable configuration corresponds to six vacancies forming "two lines," which are situated at the nearest-neighbor "out-of-plane" sites [see Fig. 3(d)]. This defect complex induces three fully occupied singlet defect states and a large number of unoccupied states, as shown in Fig. 4. For $6V_N$, we consider the (selected) 2+, 4+, and 6+ charge states, as well as the 2− and 4− negative charge states, and find that all are stable. As for the other complexes, the highest positive charge state (6+) is unbound with respect to isolated vacancies in the single positive charge state.

The total density of states of the vacancy complexes in the neutral charge state is shown in Fig. 5 (left panel), where the Fermi energy is indicated by the short black vertical line. In the right panel of Fig. 5, the total density of states for the vacancy complexes in the highest positive charge state is shown, where, in this case, the Fermi energy coincides with the valence band maximum. The defect-induced states are localized at and between the In atoms nearest to the vacancies. As an example, in Fig. 6 we show the spatial distribution of the defect states, as indicated by the label "D" in Fig.

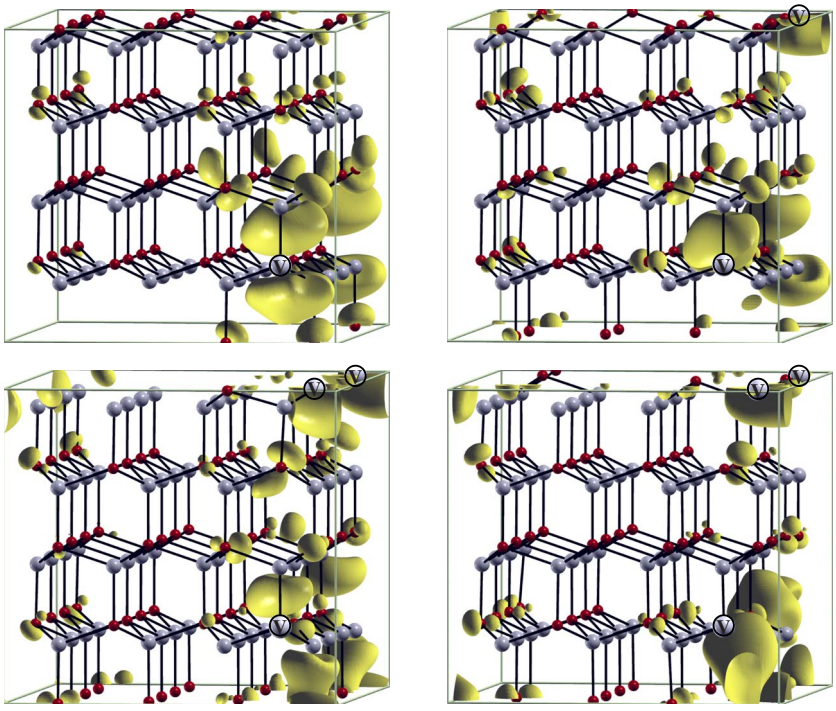

FIG. 6. (Color online) Isosurface plots of the charge density induced by the defect states (marked as D in Fig. 4) for V_N^+, $2V_N^{2+}$ (upper panel, left to right) and $3V_N^{3+}$ and $4V_N^{4+}$ (lower panel, from left to right) in the 128-atom cell. The 0.001 e/Bohr^3 isovalues are shown. The dark (red) and light gray spheres represent N and In atoms, respectively, and the open circles with "V" indicate the V_N sites.

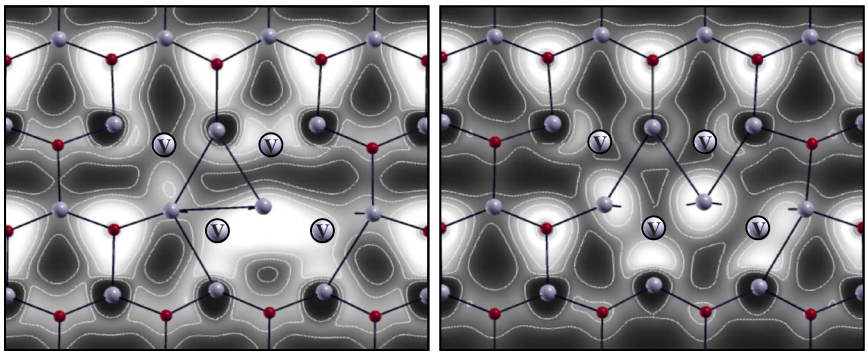

FIG. 7. (Color online) Contour plots of the ELF for the four-nitrogen vacancy cluster in the neutral (left panel) and 4– (right panel) charge states. The dark (red) and light gray spheres represent N and In atoms, respectively, and the open circles with V indicate the ideal vacancy position. The contours are drawn from 0.0 (black) to 0.8 (white) with an increment of 0.2.

4 for the nV_N configurations (where $n=1-4$) for the highest positive charge states n^+. We have carefully checked that all states lying at and between the arrows in Fig. 4 are indeed defect related states.

To investigate the character of the induced defect states and the resulting bonding in the region of the defect in more detail, we consider an electron localization function (ELF). This is a scalar function $\epsilon(\mathbf{r})$ measuring the conditional probability of finding an electron in the neighborhood of another electron with the same spin. It is expressed as[42]

$$\epsilon(\mathbf{r}) = \frac{1}{1+[D(\mathbf{r})/D_h(\mathbf{r})]^2}, \tag{3}$$

where $D(\mathbf{r})$ is the Pauli excess energy density, that is, the difference between the kinetic energy density of the system and the kinetic energy of a noninteracting system of bosons at the same density. $D_h(\mathbf{r})$ is the same quantity for the homogeneous electron gas at a density equal to the local density. According to this definition, a value of $\epsilon(\mathbf{r})$ close to 0.5 in the binding region indicates a metallic character; a value close to 1 is characteristic not only of a region where the electrons are paired to form a covalent bond but also of regions with an unpaired localized lone electron, i.e., a "dangling bond." We give an example of the ELF for $4V_N$ in the neutral and 4– charge states in Fig. 7. Here, the bright regions mean high localization (>0.8) and the dark regions indicate low localization. It is noted that in the neutral charge state there is a high localization about the In atoms neighboring the nitrogen vacancies and between the vacancies (as seen more clearly for the lower two vacancies). A high electron localization is also seen at all the N atoms, as expected. In the 4– charge state (right), the electrons are highly localized on the In atoms neighboring the nitrogen vacancies (as more clearly seen for the lower two In atoms). Similar features are found for the other nV_N vacancy complexes.

D. Formation and binding energies

We calculate the formation energies of the defects as a function of the Fermi level E_F, as shown in Fig. 8. The formation energies for the vacancy complexes are given per vacancy. It can be seen that for a *p*-type material, the single nitrogen vacancy V_N^+ has the lowest formation energy, but the formation energies of vacancy complexes and/or clusters per vacancy in the highest positive charge states are only slightly higher (practically degenerate). In more *n*-type materials, it can be seen that lower positive, neutral, and negatively charged vacancy complexes are predicted. The formation energy per vacancy of the vacancy complexes and/or clusters clearly decreases with the increasing number of vacancies for all but the highest positive charge states.

In Table II, the binding energies of the defect complexes are given per vacancy. All the calculations are performed in 128-atom supercells. As discussed earlier, it can be seen that for all charge states except the highest positive charge state for each complex, the binding energies are positive, which indicates that the interaction between vacancies is attractive. The magnitude of the binding energy per vacancy increases with the increasing number of vacancies in the complex for the neutral charge state, indicating that it is favorable to form larger clusters. For the highest positive charge states, which are present under more *p*-type conditions, all the binding

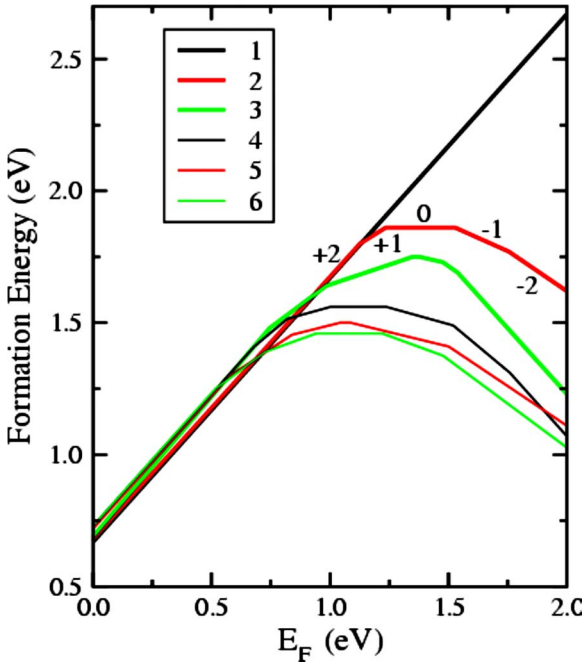

FIG. 8. (Color online) Formation energies per vacancy as a function of the Fermi level for the nitrogen vacancy and vacancy clusters in InN under In-rich conditions. The number of vacancies is listed in the legend, i.e., 1–6. The zero of the Fermi level is at the top of the valence band maximum. Kinks in the curves indicate transitions between different charge states. For example, for $2V_N$, the 2±, 1±, and neutral charge states are shown in the plots.

energies are negative, although very small, showing that the defect-clusters are unfavorable in comparison to isolated V_N^+. We note that these same trends in all the binding energies are obtained irrespective of which reference defects we use. For example, for the $5V_N^{3+}$ complex, the binding energy is positive when using any one of the following reference states: $(2\times V_N^0+3\times V_N^+)$, $(2V_N^0+3V_N^{3+})$, or $(V_N^0+4V_N^{3+})$. The fact that the N vacancies prefer to cluster together, i.e., giving local In-rich regions, could explain the reported metallic In inclusions in InN.[12]

IV. CONCLUSIONS

We have studied the electronic and structural properties and the formation energies of nitrogen vacancies in InN via first-principles density-functional theory calculations. The isolated vacancy acts as a donor in a *p*-type material where there is very little interaction between these singly positive charged vacancies. However, in more *n*-type materials, the neutral charge state becomes favored and we find that the vacancies then prefer to be situated close to one another on nearest-neighbor (like species) sites, forming "vacancy complexes or clusters." In the highest positive charge state of the complexes, clustering is unstable with respect to isolated single positive charged vacancies. However, the negatively charged and lower positively charged complexes also exhibit an attractive interaction between the vacancies, thus also favoring clustering. Such complex formation of nitrogen vacancy clusters results in a local In-rich region with a metallic-like bonding. It is possible that such structures are related to the experimentally reported In metal inclusions in InN.

ACKNOWLEDGMENTS

The authors gratefully acknowledge financial support from the Australian Research Council and supercomputing resources from the Australian Partnership for Advanced Computing National Facility and the Australian Centre for Advanced Computing and Communications.

[1] I. Vurgaftman and J. R. Meyer, J. Appl. Phys. **94**, 3675 (2003).
[2] T. Matsuoka, H. Okamoto, H. Takahata, T. Mitate, S. Mizuono, Y. Uchiyama, and T. Makimoto, J. Cryst. Growth **269**, 139 (2004).
[3] S. K. O'Leary, B. E. Foutz, M. S. Shur, and L. F. Eastman, J. Mater. Sci. **17**, 87 (2006).
[4] K. Osamura, K. Nakajima, Y. Murakami, P. H. Shingu, and A. Ohtsuki, Solid State Commun. **11**, 617 (1972).
[5] T. L. Tansley and C. P. Foley, J. Appl. Phys. **59**, 3241 (1986).
[6] V. Y. Davydov, A. A. Klochikhin, R. P. Seisyan, V. V. Emtsev, S. V. Ivanov, F. Bechstedt, J. Furthmüller, H. Harima, A. V. Mudryi, J. Aderhold, O. Semchinova, and J. Graul, Phys. Status Solidi B **229**, R1 (2002).
[7] J. Wu, W. Walukiewicz, K. M. Yu, J. W. Ager III, E. E. Haller, H. Lu, W. J. Schaff, Y. Saito, and Y. Nanishi, Appl. Phys. Lett. **80**, 3967 (2002).
[8] M. Usuda, N. Hamada, K. Shiraishi, and A. Oshiyama, Jpn. J. Appl. Phys., Part 2 **43**, L407 (2004).
[9] A. Sher, M. van Schifgaarde, M. A. Berding, S. Krishnamurthy, and A. B. Chen, MRS Internet J. Nitride Semicond. Res. **4S1**, G5.1 (1999).
[10] J. Furthmüller, P. H. Hahn, F. Fuchs, and F. Bechstedt, Phys. Rev. B **72**, 205106 (2005).
[11] P. Rinke, M. Scheffler, A. Qteish, M. Winkelnkemper, D. Bimberg, and J. Neugebauer, Appl. Phys. Lett. **89**, 161919 (2006).
[12] T. V. Shubina, S. V. Ivanov, V. N. Jmerik, D. D. Solnyshkov, V. A. Vekshin, P. S. Kop'ev, A. Vasson, J. Leymarie, A. Kavokin, H. Amano, K. Shimono, A. Kasic, and B. Monemar, Phys. Rev. Lett. **92**, 117407 (2004).
[13] C. Stampfl and C. G. Van de Walle, Phys. Rev. B **59**, 5521 (1999).
[14] C. Stampfl, C. G. Van de Walle, D. Vogel, P. Krüger, and J. Pollmann, Phys. Rev. B **61**, R7846 (2000).
[15] D. Vogel, P. Krüger, and J. Pollmann, Phys. Rev. B **55**, 12836 (1997).
[16] A. Qteish, A. I. Al-Sharif, M. Fuchs, M. Scheffler, S. Boeck, and J. Neugebauer, Phys. Rev. B **72**, 155317 (2005).
[17] R. Asahi (private communication).
[18] S. G. Louie, S. Froyen, and M. L. Cohen, Phys. Rev. B **26**, 1738 (1982).
[19] S.-H. Wei and A. Zunger, Phys. Rev. B **37**, 8958 (1988).
[20] V. Fiorentini, M. Methfessel, and M. Scheffler, Phys. Rev. B **47**, 13353 (1993).
[21] B. J. Min, C. T. Chan, and K. M. Ho, Phys. Rev. B **45**, 1159 (1992).
[22] K. S. A. Butcher, M. Wintrebert-Fouquet, P. P.-T. Chen, T. L. Tansley, H. Dou, S. K. Shrestha, H. Timmers, M. Kuball, K. E. Prince, and J. E. Bradby, J. Appl. Phys. **95**, 6124 (2004).
[23] P. Specht, R. Armitage, J. Ho, E. Gunawan, Q. Yang, X. Xu, C. Kisielowski, and E. R. Weber, J. Cryst. Growth **269**, 111 (2004).
[24] M. Yoshimoto, H. Yamamoto, W. Huang, H. Harima, J. Saraie, A. Chayahara, and Y. Horino, Appl. Phys. Lett. **83**, 3480 (2003).
[25] A. G. Bhuiyan, K. Sugita, K. Kasashima, A. Hashimoto, A. Yamamoto, and V. Y. Davydov, Appl. Phys. Lett. **83**, 4788 (2003); **84**, 452 (2004).
[26] J. Wu and W. Walukiewicz, Superlattices Microstruct. **34**, 63 (2003).
[27] A. G. Bhuiyan, A. Hashimoto, and A. Yamamoto, J. Appl. Phys. **94**, 2779 (2003).
[28] K. S. A. Butcher and T. L. Tansley, Superlattices Microstruct. **38**, 1 (2005).
[29] W. Walukiewicz, J. W. Ager III, K. M. Yu, Z. Liliental-Weber, J. Wu, S. X. Li, R. E. Jones, and J. D. Denlinger, J. Phys. D **39**, R83 (2006).
[30] J. P. Perdew and A. Zunger, Phys. Rev. B **23**, 5048 (1981).
[31] S. Baroni, A. Dal Corso, S. de Gironcoli, and P. Giannozzi, http://www.pwscf.org
[32] B. Delley, J. Chem. Phys. **113**, 7756 (2000); **92**, 508 (1990). The wave functions are expanded in terms of a double-numerical quality localized basis set with a cutoff radius of 11 Bohr. Brillouin-zone integrations are performed using a $6\times6\times4$ **k**-point Monkhorst-Pack grid.

[33] C. G. Van de Walle and J. Neugebauer, J. Appl. Phys. **95**, 3851 (2004).

[34] *Properties of Group-III Nitrides*, edited by J. H. Edgar, EMIS Datareviews Series (IEE, London, 1994).

[35] M. Fuchs, J. L. F. Da Silva, C. Stampfl, J. Neugebauer, and M. Scheffler, Phys. Rev. B **65**, 245212 (2002).

[36] *CRC Handbook of Chemistry and Physics*, 77th ed., edited by D. R. Lide (CRC, Boca Raton, FL, 1997).

[37] S. I. Simak, U. Haussermann, R. Ahuja, S. Lidin, and B. Johansson, Phys. Rev. Lett. **85**, 142 (2000).

[38] The lattice constant of bulk In as described in the nlcc approach is smaller than the corresponding value obtained with inclusion of the *d* states [see, e.g. M. Fuchs, J. L. F. Da Silva, C. Stampfl, J. Neugebauer, and M. Scheffler, Phys. Rev. B **65**, 245212 (2002)]. However, for consistency with our treatment of In for InN, we used the same approach in order to maximize error cancellation. We verified that atomic relaxations about a number of defects in InN are consistent with the all-electron approach of the DMOL^3 code: For the nitrogen vacancy in the neutral (1+) charge state, all-electron and nlcc approaches yield −1.7% (−0.5%) and −3.2% (−1.8%) changes for the neighboring In atoms, respectively. For clustering of two nitrogen vacancies in the neutral charge states, all-electron and nlcc approaches yield −4.9% and −6.9% changes for the neighboring In atoms, respectively. For the neutral indium vacancy, all-electron and nlcc approaches yield 8.7% and 6.7% changes of the surrounding N atoms, respectively.

[39] C. Kittel, *Introduction to Solid State Physics* (Wiley, New York, 1986).

[40] R. W. G. Wyckoff, *Crystal Structures* (Wiley, New York, 1963), Vol. I.

[41] By using the DMOL^3 code and the generalized-gradient approximation, the obtained values of the binding energy of the (neutral) nitrogen vacancies per vacancy for $2V_N$, $3V_N$, and $4V_N$ are 0.060, 0.185, and 0.261 eV, respectively. For these calculations, the wave functions are expanded in terms of a double-numerical quality localized basis set with a cutoff radius of 11 Bohr and a **k**-point sampling of $3\times3\times3$ in a 96-atom supercell.

[42] A. Savin, O. Jepsen, J. Flad, O. K. Andersen, H. Preuss, and H. G. Von Schneiring, Angew. Chem. Int. Ed. Engl. **31**, 187 (1992).